Crystalline Silicon Nanotubes and Their Connections with Gold Nanowires in Both Linear and Branched Topologies

Bensong Chen, Guowen Meng,* Qiaoling Xu, Xiaoguang Zhu, Mingguang Kong, Zhaoqin Chu, Fangming Han, and Zhuo Zhang

Key Laboratory of Materials Physics, and Anhui Key Laboratory of Nanomaterials and Nanostructures, Institute of Solid State Physics, Chinese Academy of Sciences, Hefei, Anhui 230031, P. R. China

ABSTRACT Silicon, being in the same group in the periodic table as carbon, plays a key role in modern semiconductor industry. However, unlike carbon nanotube (NT), progress remains relatively slow in silicon NT (SiNT) and SiNT-based heteroarchitectures, which would be the fundamental building blocks of various nanoscale circuits, devices, and systems. Here, we report the synthesis of linear and branched crystalline SiNTs *via* porous anodic aluminum oxide (AAO) self-catalyzed growth and postannealing, and the connection of crystalline SiNTs and gold nanowires (AuNWs) *via* a combinatorial process of electrodepositing AuNWs with predesired length and location in the channels of the AAO template and subsequent AAO self-catalyzed and postannealing growth of SiNTs in the remaining empty channels adjacent to the AuNWs. Using the approach, a large variety of two-segment AuNW/SiNT and three-segment SiNT/AuNW/SiNT heteronanostructures with both linear and branched topologies have been achieved, paving the way for the rational design and fabrication of SiNT-based nanocircuits, nanodevices, and multifunctional nanosystems in the future.

KEYWORDS: silicon nanotubes · gold nanowires · interconnected heterostructures · linear and branched topologies

Since the discovery of carbon nanotube (CNT),[1] considerable attention has been attracted owing to its fascinating molecular structures with attractive electronic,[2] thermal,[3] chemical,[4] and mechanical[5] properties. Many routes have been exploited for the synthesis of CNTs,[6] and in the mean time CNT-based heteroarchitectures have been constructed as building blocks of various nanoscale devices, including two-segment heterostructures of semiconductor nanowire (NW) and CNT,[7−9] semiconductor nanotube (NT) and CNT,[10] metal NW and CNT,[11] and three-segment heterostructures of CNT, metal NW, and CNT.[12,13] Silicon, being in the same group in the periodic table as carbon, plays a key role in modern semiconductor industry and device fabrication. Theoretical studies predict that stable silicon NTs (SiNTs) would exhibit semiconducting features[14] and may have potential applications in magnetics,[15] photoelectronics,[16] electronic transport,[17] and hydrogen storage.[18] However, unlike metal nanocluster-catalyzed vapor−liquid−solid (VLS) growth of CNTs,[19] little has been reported on the growth of SiNTs *via* the VLS approach owing to the favorable formation of sp^3 hybridization of silicon, leading to Si NWs rather than SiNTs.[20] Therefore, progress remains relatively slow in the synthesis of SiNTs. Up to now, various approaches have been tried for SiNTs.[21−26] Among them, porous anodic aluminum oxide (AAO) template-assisted routes are most studied. First, Au nanoclusters were decorated on the inner pore walls of the porous AAO template for catalytic growth of SiNTs.[22] However, the resultant products were a mixture of SiNTs and SiNWs rather than pure SiNTs as the base of some pores is closed with Au film, leading to VLS growth of SiNWs. In addition, some of the predecorated Au clusters on the pore walls were embedded in the SiNTs, resulting in the contamination of the SiNTs. Then, molecular beam epitaxy on a porous AAO template was used to synthesize SiNTs without using catalysts;[23] however, the SiNTs grew from the pore edge on top of the AAO template rather than inside the pores, therefore the SiNTs were very short. Afterward, AAO-assisted multistep replication in a chemical vapor deposition (CVD) process was used to synthesize SiNTs;[24] however, the fabrication process is very complicated as an AAO template consisting of annular nanochannels with NiO NW cores has to be achieved first, and then Ni atoms on the NiO NW core surface catalyze the decomposition of silane to form SiNTs under the annular nanochannel geometrical confinement. Subsequently, SiNTs would be achieved after removing the AAO template and the inner NiO NW cores. However, there remain residual NiO NW cores inside the SiNTs,

*Address correspondence to gwmeng@issp.ac.cn.

Received for review April 27, 2010 and accepted November 04, 2010.

Published online November 16, 2010.
10.1021/nn102689z

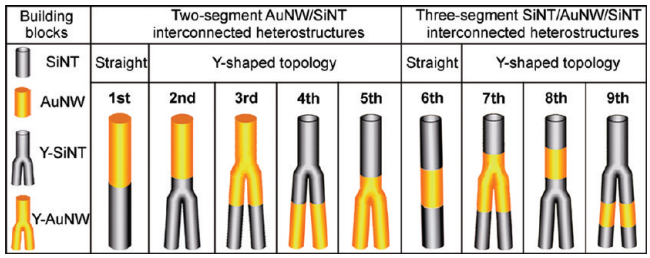

Figure 1. Schematics showing a catalogue of two-segment AuNW/SiNT and three-segment SiNT/AuNW/SiNT interconnected heterostructures with both linear and branched topologies. The left column presents the building blocks, where SiNT and Y-SiNT stand for straight and Y-shaped SiNT (hollow in shape and dark in color), and AuNW and Y-AuNW stand for straight and Y-shaped AuNW (solid in shape and yellow in color), respectively. The ordinal number designates each of the architectures. The nine types of architectures are categorized according to the number of hybrid segments in the axial direction and the topology: two-segment AuNW/SiNT heterostructures with linear (the 1st one) and Y-shaped (from the 2nd to the 5th ones) topologies, and three-segment SiNT/AuNW/SiNT heterostructures with linear (the 6th one) and Y-shaped (from the 7th to 9th ones) topologies.

also leading to the contamination of the SiNTs. Therefore, exploiting an easy and controllable synthetic approach to crystalline SiNTs without any contamination is a great challenge. Furthermore, nothing is reported on the connections of SiNTs and NWs, which are ultimately central to the rational design of building blocks for SiNT-based nanodevices and nanosystems. Up to now, several localized joining methods, such as laser heating[27] and nanowelding[28] techniques, have been used for assembling individual nano-objects into complex nanostructures. However, these methods are costly, time-consuming, and only one nanojunction could be constructed each time. Herein, using a similar synthetic approach to that of AAO template-assisted growth of CNTs without using any catalysts,[29] we report the synthesis of straight and branched polycrystalline SiNTs without contamination *via* porous AAO template self-catalyzed growth and postannealing. The process continues with the connecting of the straight and branched SiNTs with Au NWs *via* sequential electrochemical depositing (ECD) of AuNWs with predesired length and location in the nanochannels of the AAO template and the AAO self-catalyzed and postannealing growth of SiNTs in the remaining channels adjacent to the AuNWs. Using the approach, a wide variety of two-segment AuNW/SiNT and three-segment SiNT/AuNW/SiNT heteronanostructures with both linear and branched topologies, as shown schematically in Figure 1, has been achieved, which might have promising potential as fundamental building blocks for SiNT-based nanocircuits, nanodevices, and nanosystems.

RESULTS AND DISCUSSION

First, we tried to grow SiNTs inside bare native nanochannels of AAO templates using a CVD process much similar to that of AAO self-catalyzed growth of CNTs without any catalysts.[29] Herein, silane (SiH_4) rather than acetylene (C_2H_2) was used as precursor and heated at 500 °C for pyrolysis to obtain the Si species. In the CVD process, we used two kinds of porous AAO as templates: one with straight channels and the other with branched (*e.g.*, Y-shaped) channels, respectively. As expected, transmission electron microscopy (TEM) observations (Figure 2 panels A and B) reveal that tube-like nanostructures with straight and Y-shaped morphologies were achieved accordingly after the AAO templates removal. For the straight SiNTs, the outer diameter is about 70−80 nm, while for the Y-shaped SiNTs the outer diameters of the stem and the branched segments are about 80 and 45 nm, respectively, indicating that the resultant tube-like Si nanostructures replicate

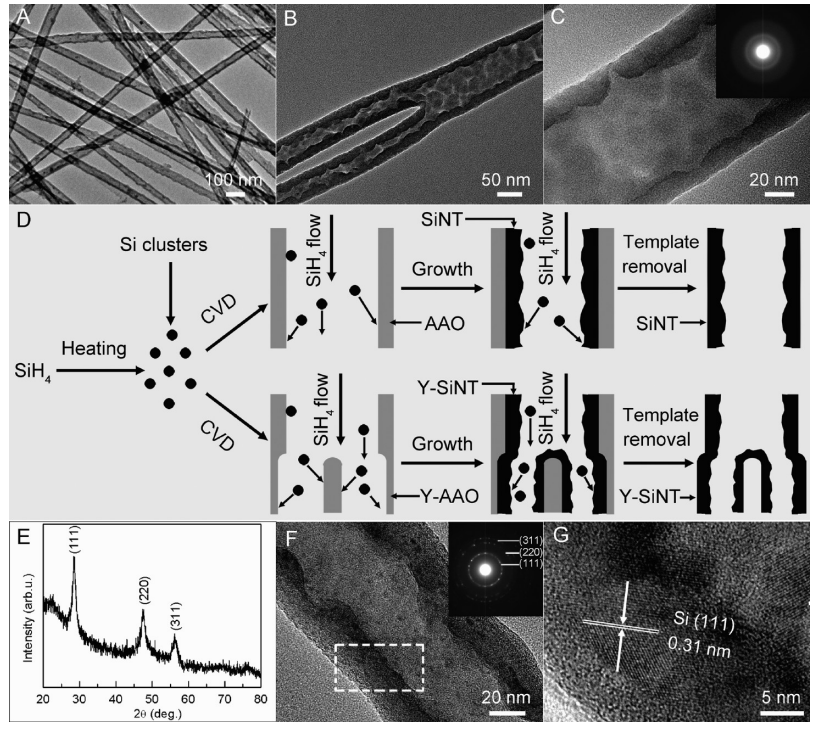

Figure 2. TEM images of (A) straight and (B) Y-shaped SiNTs achieved inside the AAO templates with corresponding shaped channels, respectively. (C) Enlarged TEM image of a straight pristine SiNT; inset is its corresponding SAED pattern. (D) Schematics of the amorphous SiNTs formation in both straight (top) and Y-shaped (bottom) nanochannels. (E) XRD pattern of the postannealed SiNTs. (F) Enlarged TEM image of a single postannealed SiNT, inset is the corresponding SEAD pattern. (G) HRTEM image of wall region (taken from the dotted-line rectangle area in panel F) of the postannealed SiNT.

the geometrical morphology and the size of the native nanochannels of the AAO templates. TEM image of a single straight SiNT (Figure 2C) shows that the wall thickness of the SiNT is about 15−20 nm, and a selected area electron diffraction (SAED) pattern taken on the SiNT (inset in Figure 2C) displays typical noncrystalline diffraction rings, demonstrating that the SiNTs achieved *via* porous AAO self-catalyzed growth are amorphous. The growth mechanism of the amorphous SiNTs inside the AAO templates with straight and Y-shaped nanochannels is schematically shown in Figure 2D. We assume that the inner pore walls of the porous AAO templates have uniform catalytic action in the CVD process, thus when gaseous SiH_4 precursor flows into the native channels of the AAO template, SiH_4 pyrolysis occurs to form Si clusters that spread over the pore wall surfaces. The upcoming Si clusters from the continuous decomposition of SiH_4 will randomly accumulate on the internal pore walls, leading to the formation of tube-like amorphous Si nanostructures under the geometrical confinement of the native nanochannels inside the AAO templates.

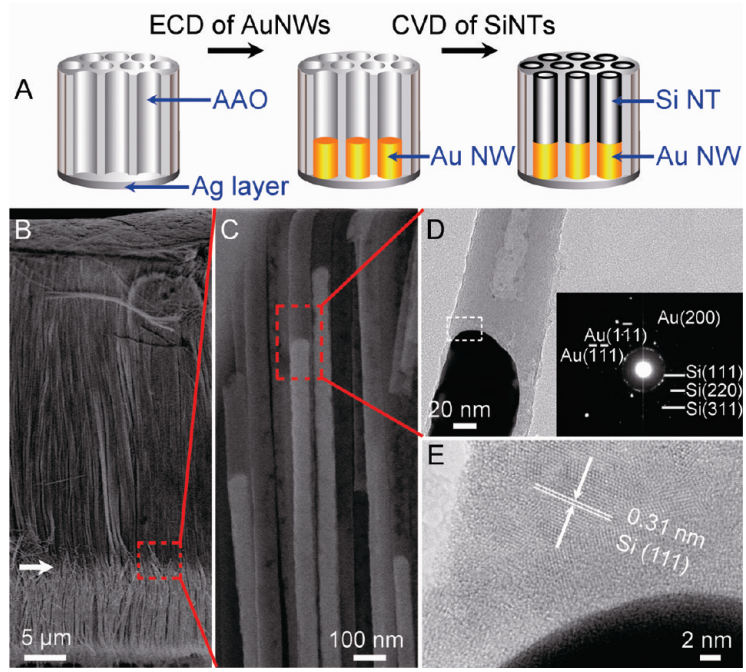

Figure 3. AuNW/SiNT heterostructures in linear topology. (A) Schematic fabrication procedure; (B) side-view SEM image of a bundle of the AuNW/SiNT heterostructures after template removal; (C) close-up SEM image of the AuNW/SiNT junction area (marked with white arrow in panel B); (D) TEM and (E) HRTEM (taken from the dotted-line rectangle area in panel D) images of the AuNW/SiNT junction. The inset in panel D is the SAED pattern from the dotted-line rectangle area in panel D.

We then tried to enhance the crystallinity of the AAO self-catalyzed-grown amorphous SiNTs *via* postannealing at 750 °C for 2 h in Ar/H_2 atmosphere. Typical X-ray diffraction (XRD) pattern of the postannealed SiNTs (Figure 2E) shows diffraction peaks indexed to diamond-like cubic silicon with a lattice constant of $a = 0.54$ nm, being consistent with the standard value of cubic silicon (JCPDS file 27-1402: $a = 0.5430$ nm). Enlarged TEM image of a single postannealed SiNT (Figure 2F) demonstrates that the tubular structure of the SiNT is maintained after annealing. The SAED pattern of the postannealed SiNT (inset in Figure 2F) displays the sharp polycrystalline diffraction rings with spotlike features, referring to (111), (220), and (311) planes of cubic phase Si. Lattice-resolved TEM image of the tube wall of the postannealed SiNT (Figure 2G) clearly shows visible lattice fringes of (111) planes of Si, further confirming the transformation of the SiNT from amorphous to polycrystalline nature after being postannealed. As not any catalyst is introduced in the process, highly polycrystalline SiNTs without contamination have been achieved in the native nanochannels of the AAO template by AAO self-catalyzed growth and postannealing. It should be noted that the crystalline quality of the SiNTs could be further improved by using a higher postannealing temperature, and the electronic properties of the SiNTs could be tailored by p-type or n-type doping *via* mixing gaseous borane or phosphine in the CVD process.

Connecting SiNTs with NWs to construct SiNT-based hybrid nanoheterostructures is crucial to the design of building blocks for nanocircuits, nanodevices, and nanosystems. Gold (with excellent conductivity and stability in the oxidizing environment) is widely used in microelectronic devices, and AuNWs can be achieved in the nanochannels of the AAO template *via* electrodeposition.[30] Here, we tried to connect AuNW and straight SiNT to achieve two-segment AuNW/SiNT and three-segment SiNT/AuNW/SiNT heterostructures with linear topology.

For two-segment AuNW/SiNT heteroarchitectures (the first architecture in Figure 1), a combinatorial process was applied as shown in Figure 3A schematically. First, a AuNWs segment is electrodeposited inside half channels of the straight-channel AAO template coated with a thin silver (Ag) film as an electrode for the ECD, and then AAO self-catalyzed and postannealing growth of the polycrystalline SiNT segment is applied in the remaining empty channels adjacent to the AuNWs. Side-view scanning electron microscopy (SEM) image of a bundle of the AuNW/SiNT heterostructures (Figure 3B) after the template removal shows one sharp interface (marked with white arrow) between the dark contrast SiNTs segment (see energy-dispersive X-ray spectroscopy (EDS) analysis in Supporting Information, Figure S1A) and the light contrast AuNWs segment (see Figure S1B). A close-up SEM view of the interfaces between AuNWs and SiNTs (Figure 3C) clearly displays that the

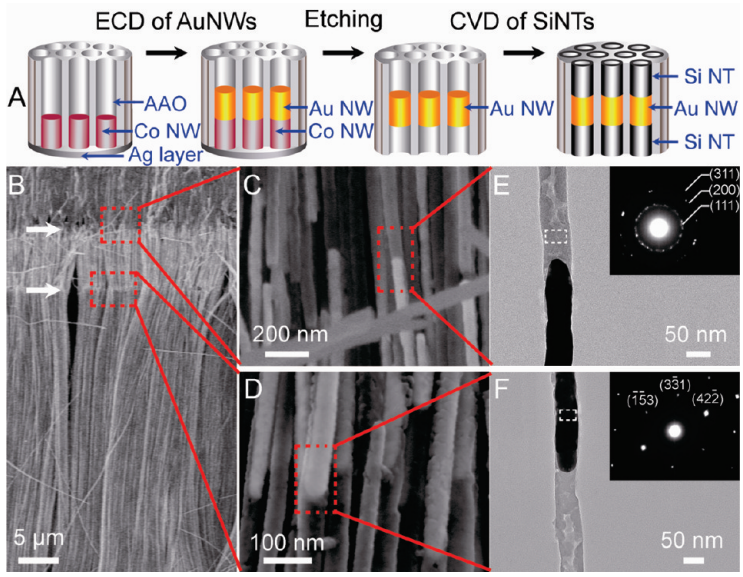

Figure 4. Three-segment SiNT/AuNW/SiNT heterostructures in linear topology: (A) schematic fabrication procedure; (B) side-view SEM image of a bundle of the SiNT/AuNW/SiNT heterostructures after template removal; (C, D) close-up SEM images of the (C) SiNT/AuNW and (D) AuNW/SiNT junction area (located on the upper and lower parts and marked with white arrows in panel B, respectively); (E, F) TEM images of typical (E) SiNT/AuNW and (F) AuNW/SiNT junctions of the heterostructure. The insets in panels E and F are SAED patterns from the AuNW and SiNT segments. respectively, taken on the dotted-line rectangle areas.

AuNWs and SiNTs are well connected. Enlarged TEM image of a typical AuNW/SiNT junction (Figure 3D) shows that the AuNW is closely capped with the SiNT, confirming that good adherence between SiNT and AuNW has been achieved. The SAED pattern taken on the junction part (inset in Figure 3D) displays obvious diffraction rings for the SiNT segment and diffraction spots for the AuNW, respectively, revealing the polycrystalline nature of the SiNT segment and the single-crystalline nature of the AuNW segment. A lattice-resolved TEM image taken on the AuNW/SiNT junction area (Figure 3E) shows lattice-fringes of the SiNT segment with a lattice space of about 0.31 nm which corresponds to the (111) planes of Si, further confirming the polycrystalline nature of the SiNT. It is noticed that the AuNW/SiNT junction interface (Figure 3E) is not quite abrupt, which could be ascribed to the interdiffusion and reconstruction of Au and Si atoms at the Au/Si interface during postannealing. The XRD spectrum of the resultant AuNW/SiNT heterostructures (see Supporting Information Figure S2) reveals that all of the sharp peaks can be indexed to diamond-like cubic silicon (JCPDS file 27-1402) and face-centered cubic Au (JCPDS file 04-0784). Taken together, polycrystalline SiNTs have been longitudinally connected with single crystalline AuNWs to form two-segment AuNW/SiNT heterostructures in linear topology.

For three-segment SiNT/AuNW/SiNT heterostructures (the sixth architecture in Figure 1), a combinatorial process was applied as shown schematically in Figure 4A. A segment of sacrificial metallic NWs (*e.g.*, cobalt NWs, CoNWs) and desired AuNWs are sequentially electrodeposited into the bottom half channels of the AAO template, then selective wet chemical etching of the Ag electrode and the sacrificial CoNWs is carried out to force the AuNWs to embed in the middle of the channels leaving the two ends empty. Finally, the AAO self-catalyzed and postannealing growth of SiNTs on both ends of the AuNW segments in the empty channels leads to linear three-segment SiNT/AuNW/SiNT heterostructures. SEM observation on a bundle of the resultant products shows the overall morphology of the linear three-segment SiNT/AuNW/SiNT heterostructures (Figure 4B), and the enlarged images (Figure 4 panels C and D) reveal that the interfaces between SiNT and AuNW are well adhered. TEM images (Figure 4 panels E and F) of a typical AuNW/SiNT junction area further demonstrate that SiNT and AuNW are well connected. The SAED patterns taken on the SiNT (the inset in Figure 4E) and AuNW (the inset in Figure 4F) segments demonstrate the polycrystalline nature of SiNT and single-crystalline nature of AuNW, respectively.

If AAO with branched channels is used as a template, AuNW and SiNT can also be connected to form AuNW/SiNT and SiNT/AuNW/SiNT heterostructures with branched topology, which will open up the opportunities for constructing three-dimensionally interconnected complex nanocircuits. For simplicity, we will demonstrate Y-branched topology in the following, while one can easily extend the approach for multiple branched topologies.[31]

For AuNW/SiNT heterostructures with Y-branched topology, four types of connections (from the second to the fifth architectures) can be achieved as shown schematically in Figure 1. We will detail the case for AuNW/Y-SiNT heterostructures (the second architecture in Figure 1) where a straight AuNW longitudinally connects with the stem end of a Y-shaped SiNT (Y-SiNT). Figure 5A schematically shows the fabrication process of the AuNW/Y-SiNT heterostructures. First, a short straight segment of AuNWs is electrodeposited into the bottom part of the stem channels of the Y-shaped-channel AAO (Y-AAO) template with a silver layer coated on the planar surface of the stem-channel side. Then, AAO self-catalyzed and postannealing growth of SiNTs is carried out inside the remaining empty Y-shaped channels adjacent to the AuNWs to form the Y-SiNT segment. The side-view SEM image of a bundle of the AuNW/Y-SiNT heterostructures after the template removal (Figure 5B) shows a sharp interface (located on the upper part and marked with white arrow) between the light contrast AuNW segments and the dark contrast SiNT segments, and another interface (located on the lower part and marked with red arrow) where the Y-branchings of SiNTs take place. The enlarged SEM

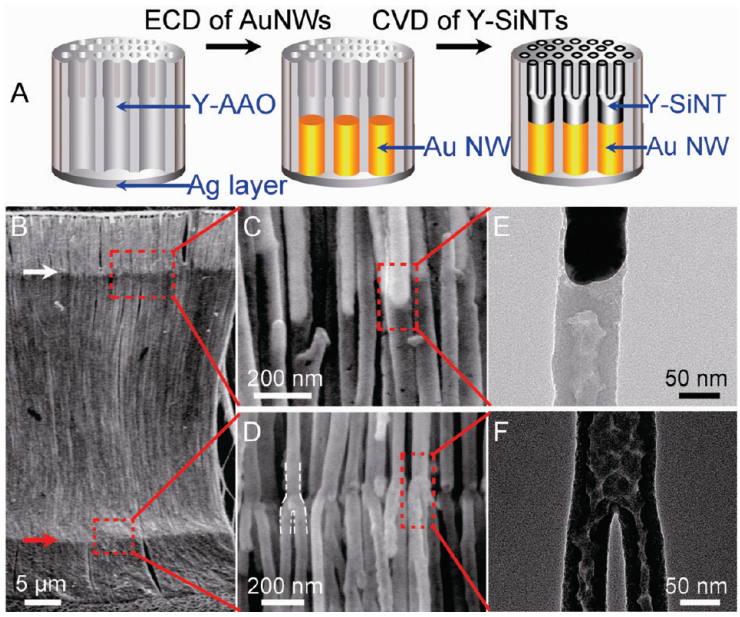

Figure 5. AuNW/Y-SiNT heterostructures with Y-shaped topology. (A) Schematic fabrication procedure; (B) side-view SEM image of a bundle of the AuNW/Y-SiNT heterostructures after template removal; (C, D) close-up SEM images of the corresponding (C) AuNW/SiNT junction area and (D) Y-branchings of Y-SiNTs (marked with white and red arrows in panel B, respectively). The Y-junction in panel D is contoured in a white dotted line for clarity. (E, F) TEM images of the typical (E) AuNW/SiNT junction and (F) Y-SiNT of the heterostructure.

image of AuNW/SiNT junction region (Figure 5C) reveals that longitudinally connected AuNWs and SiNTs in the stems have the same diameter. A close-up SEM view of the Y-branching interface (Figure 5D) verifies the Y-shaped morphology of the SiNTs. TEM image (Figure 5E) of a typical AuNW/SiNT junction further confirms that the AuNW and SiNT are well connected. TEM image taken on the Y-junction area of the Y-SiNT (Figure 5F) shows that the stem and the branches of the Y-SiNT have diameters of about 80 and 45 nm, respectively, in agreement with those of the Y-shaped channels inside the AAO templates. Taken together, well-interconnected AuNW/Y-SiNT heterostructures have been achieved. If the electrodeposition process lasts longer, the AuNWs will go beyond the Y-junction to form Y-shaped AuNWs (Y-AuNWs) and still leave some channels near the end of branched side empty. After AAO self-catalyzed and postannealing growth of SiNTs in the remaining empty channels, Y-AuNW/2SiNTs heterostructures (the third architecture in Figure 1, *i.e.*, one Y-shaped AuNW longitudinally connects with two straight parallel SiNTs in the ends of two branches of the Y construct) would be achieved (see Supporting Information Figure S3).

On the contrary, if the electrodeposition of AuNWs is carried out from the planar surface of the branched-channel side of the Y-AAO template, straight AuNWs and Y-shaped AuNWs can be grown in part sections of the Y-shaped channels, and subsequently filling the remainder of the empty nanochannels with SiNTs will result in Y-SiNT/2AuNWs heterostructures (the fourth architecture in Figure 1, one Y-shaped SiNT longitudinally connects with two parallel AuNWs in the two branches of the Y construct, see Supporting Information Figure S4) and SiNT/Y-AuNW heterostructures (the fifth architecture in Figure 1, one SiNT longitudinally connects with the stem end of a Y-shaped AuNW, see Supporting Information Figure S5), respectively.

Following the rationale of connecting three-segment SiNT/AuNW/SiNT heteroarchitectures in linear channels of an AAO template, three types of three-segment SiNT/AuNW/SiNT connections with Y-branched topology could be achieved (see the seventh to the ninth architectures in Figure 1). We will take the seventh architecture (SiNT/Y-AuNW/2SiNTs heterostructures, *i.e.*, one SiNT longitudinally connects with the stem end of a Y-shaped AuNW, and sequentially connects with another two parallel SiNTs in the branches of the Y-shaped AuNWs) as an example. The fabrication process is shown schematically in Figure 6A. First, a short straight sacrificial segment of CoNWs and predesigned Y-shaped AuNWs are sequentially electrodeposited beyond the Y-junction region of the Y-AAO template, still leaving a portion of branched channels near the template planar surface empty. Then selective wet chemical etching of the Ag layer and the sacrificial CoNWs segment forces the Y-AuNWs to be located at the Y-junction region of the channels with both end channel sections empty. Subsequent filling of the remaining empty nanochannels on both ends of the Y-AuNWs with polycrystalline SiNTs results in SiNT/Y-AuNW/2SiNTs heterostructures. A side-view SEM image (Figure 6B) displays the overall morphology of the SiNT/Y-AuNW/2SiNTs heterostructures after template removal. EDS analyses on each segment of the SiNT/Y-AuNW/2SiNTs heterostructures (see Supporting Information Figure S6) reveal that the main compositions of the three segments are Si, Au, and Si, respectively. Enlarged SEM images of the AuNW/SiNT interface (Figure 6C) and Y-branchings of the Y-AuNWs (Figure 6D) verify that SiNTs and the stem of Y-AuNWs are well adhered. TEM image of a typical AuNW/SiNT junction (Figure 6E) clearly shows the good adherence between AuNW and SiNT. The Y-shaped topology of AuNWs segment can be verified in the TEM image taken on the Y-junction area (Figure 6F).

By electrodepositing the AuNWs in the middle of either stem channels or branched channels, heterostructures of SiNT/AuNW/Y-SiNT (the eighth architec-

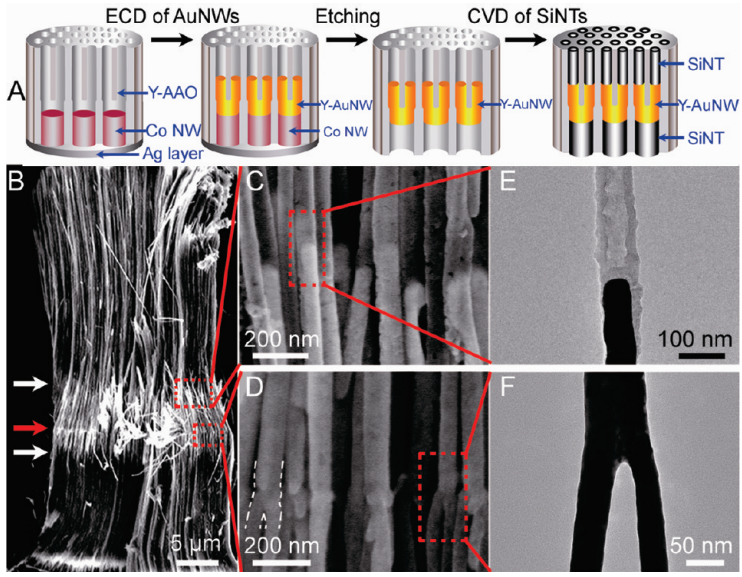

Figure 6. SiNT/Y-AuNW/2SiNTs heterostructures with Y-shaped topology: (A) schematic fabrication procedure; (B) side-view SEM image of a bundle of the SiNT/Y-AuNw/2SiNTs heterostructures after template removal; (C, D) close-up SEM images of (C) AuNW/SiNT junction area and (D) Y-branchings of Y-AuNWs (marked with white and red arrows in panel B, respectively). The Y-junction in panel D is contoured in the white dotted line for clarity. (E, F) TEM images of the typical (E) AuNW/SiNT junction and (F) Y-AuNW of the heterostructure.

ture in Figure 1, *i.e.*, one SiNT longitudinally connects with an AuNW of the same diameter, and sequentially connects with the stem end of a Y-shaped SiNT) or Y-SiNT/2AuNWs/2SiNTs (the ninth architecture in Figure 1, *i.e.*, one Y-shaped SiNT longitudinally connects with two parallel AuNWs in the branches of Y-construct, and sequentially connects with another two parallel SiNTs with the same diameter in the branches again) could be achieved. For example, SiNT/AuNW/Y-SiNT connections have been achieved (see Supporting Information Figure S7).

The Y-shaped topologies of the heterostructures can also be extended to multiple branches if AAO with multiple branched channels[31] is used as templates in our fabrication process. For example, by using an AAO template with three-branched nanochannels, three-branched-SiNT/3AuNWs architectures (*i.e.*, one three-branched SiNT longitudinally connects with three AuNWs in the ends of their three branches) have been achieved (see Supporting Information Figure S8).

The as-fabricated two-segment AuNW/SiNT and three-segment SiNT/AuNW/SiNT heterostructures with both linear and branched topologies enable the connection of crystalline SiNTs with single crystalline AuNWs for constructing SiNT-based prototype nanocircuits with distinct morphologies and well-connected nanoscale contact. Especially, the Y- and multibranched heterostructures can be used as functional prototype nanocircuits with a one-input structure yielding corresponding two-output and multioutput complex structures, respectively, providing the opportunities for design of nanoscale logic gates[32] and electronic rectifiers[33] by using the branched units. Compared with the localized joining methods reported previously for assembling individual nanoscale objects into complex nanostructures and nanocircuits,[27,28] our approach for the synthesis of AuNW/SiNT heterostructures provides an effective, low-cost, and easy way to control the morphology and the assembling mode of the nanostructures, paving the way for the design of SiNT-based prototype nanocircuits with potential applications in functional nanodevices.

CONCLUSIONS

We have demonstrated the synthesis of polycrystalline SiNTs with both linear and branched topologies *via* porous AAO self-catalyzed and postannealing growth. We have also shown the connection of the polycrystalline SiNTs with single crystalline AuNWs *via* a combinatorial process of electrodepositing sacrificial CoNWs and the desired AuNWs in predesigned portions of the nanochannels of the porous AAO template, which then underwent selective wet chemical etching of the sacrificial NW segment near the planar surface of the template and AAO self-catalyzed and postannealing growth of crystalline SiNTs in the remaining empty channels on the ends of AuNWs. Using this approach, a wealth of two-segment AuNWs/SiNT and three-segment SiNT/AuNW/SiNT connections with both linear and branched topologies were achieved. These SiNT-based two-segment and three-segment heteronanostructures with both linear and branched topologies will pave the way for the design and fabrication of spatially interconnected SiNT-based nanocircuits, nanodevices, and multifunctional nanosystems.

METHODS

AAO Template Preparation. The AAO templates with straight nanochannels were synthesized by a two-step anodizing process reported elsewhere[34] (anodized at 50 V in oxalic acid at 10 °C, the pore diameter is about 70−80 nm). Y-AAO templates were obtained in 0.3 M oxalic acid under anodized voltages of 50 V for stems and 35 V for branches at 10 °C.[31] AAO templates with three-branched-channels were achieved in 0.3 M oxalic acid under anodized voltages of 60 V for stems and 34.6 V for branches at 3 °C, respectively.[31]

Electrochemical Deposition of Au and Co NWs. The electrodeposition of CoNWs[35] and AuNWs[30] was performed under a constant current density of 1.0 mA cm^{-2} and 10 μA cm^{-2} at room temperature, respectively.

Selective Wet Chemical Etching of the Ag Layer and the Sacrificial CoNWs. The sputtered Ag film and sacrificial CoNWs were selectively etched by using concentrated nitric acid.

AAO Self-Catalyzed and Postannealing Growth of Crystalline SiNT Segments. The growth of SiNTs in remaining empty nanochannels of AAO templates was carried out in a horizontal quartz

tube furnace under atmospheric pressure. Preliminarily, the as-prepared AAO template embedded with AuNWs was placed in a ceramic boat in the center of quartz tube, and then the system was purged by high purity N_2 flow for 3 h. Afterward, a constant mixture gas flow of N_2 (100 sccm) and H_2 (15 sccm) was introduced and maintained during both heating and cooling stages. The temperature of the tube furnace was raised to a peak temperature of 500 °C at a rate of 10 °C/min and then pure silane was injected into the furnace and maintained for 2.5 h at a flow rate of 3.5 sccm. After the growth of the SiNTs, *in situ* annealing was performed at 750 °C for 2 h in a mixed gas flow of Ar (85 sccm) and H_2 (15 sccm).

Structural Characterizations. The as-prepared samples were carefully polished with sandpaper to remove the additional deposits on the planar surfaces of the AAO template, then immersed in concentrated HCl solution at 85 °C for 5 h to remove the AAO templates, and finally cleaned with deionized water thoroughly. The resultant heterostructures were dispersed in anhydrous ethanol and characterized by using X-ray diffraction (XRD, Philips, X'Pert Pro MPD, with Cu Kα irradiation), scanning electron microscopy (SEM, Sirion 200, FEI, at 5 kV) with energy-dispersive X-ray spectroscopy (EDS OXFORD), transmission electron microscopy, and high-resolution TEM (HRTEM, JEOL2010 at 200 kV).

Acknowledgment. This work was supported by National Natural Science Foundation of China (Grant No. 50525207, 50972145), and National Basic Research Program of China (Grant No. 2007CB936601).

Supporting Information Available: EDS analyses on the resultant AuNW/SiNT and SiNT/Y-AuNW/2SiNTs heterostructures, XRD characterizations of postannealed AuNW/SiNT heterostructures, schematic fabrication procedures, and morphological characterizations for Y-AuNW/2SiNTs, Y-SiNT/2AuNWs, SiNT/Y-AuNW, SiNT/AuNW/Y-SiNT and three-branched-SiNT/3AuNWs heterostructures with branched topologies, respectively. This material is available free of charge *via* the Internet at http://pubs.acs.org.

REFERENCES AND NOTES

1. Iijima, S. Helical Microtubules of Graphitic Carbon. *Nature* **1991**, *354*, 56–58.
2. Engel, M.; Small, J. P.; Steiner, M.; Freitag, M.; Green, A. A.; Hersam, M. C.; Avouris, P. Thin Film Nanotube Transistors Based on Self-Assembled, Aligned, Semiconducting Carbon Nanotube Arrays. *ACS Nano* **2008**, *2*, 2445–2452.
3. Biercuk, M. J.; Llaguno, M. C.; Radosavljevic, M.; Hyun, J. K.; Johnson, A. T.; Fischer, J. E. Carbon Nanotube Composites for Thermal Management. *Appl. Phys. Lett.* **2002**, *80*, 2767–2769.
4. Claussen, J. C.; Franklin, A. D.; ul Haque, A.; Porterfield, D. M.; Fisher, T. S. Electrochemical Biosensor of Nanocube-Augmented Carbon Nanotube Networks. *ACS Nano* **2009**, *3*, 37–44.
5. Cadek, M.; Coleman, J. N.; Barron, V.; Hedicke, K.; Blau, W. J. Morphological and Mechanical Properties of Carbon-Nanotube-Reinforced Semicrystalline and Amorphous Polymer Composites. *Appl. Phys. Lett.* **2002**, *81*, 5123–5125.
6. Awasthi, K.; Srivastava, A.; Srivastava, O. N. Synthesis of Carbon Nanotubes. *J. Nanosci. Nanotechnol.* **2005**, *5*, 1616–1636.
7. Hu, J. T.; Ouyang, M.; Yang, P. D.; Lieber, C. M. Controlled Growth and Electrical Properties of Heterojunctions of Carbon Nanotubes and Silicon Nanowires. *Nature* **1999**, *399*, 48–51.
8. Zhang, Y.; Ichihashi, T.; Landree, E.; Nihey, F.; Iijima, S. Heterostructures of Single-Walled Carbon Nanotubes and Carbide Nanorods. *Science* **1999**, *285*, 1719–1722.
9. Yan, X. B.; Tay, B. K.; Miele, P. Field Emission from Ordered Carbon Nanotube−ZnO Heterojunction Arrays. *Carbon* **2008**, *46*, 753–758.
10. Liao, L.; Liu, K. H.; Wang, W. L.; Bai, X. D.; Wang, E. G.; Liu, Y. L.; Li, J. C.; Liu, C. Multiwall Boron Carbonitride/Carbon Nanotube Junction and Its Rectification Behavior. *J. Am. Chem. Soc.* **2007**, *129*, 9562–9563.
11. Sun, S. H.; Yang, D. Q.; Zhang, G. X.; Sacher, E.; Dodelet, J. P. Synthesis and Characterization of Platinum Nanowire−Carbon Nanotube Heterostructures. *Chem. Mater.* **2007**, *19*, 6376–6378.
12. Ou, F. S.; Shaijumon, M. M.; Ci, L. J.; Benicewicz, D.; Vajtai, R.; Ajayan, P. M. Multisegmented One-Dimensional Hybrid Structures of Carbon Nanotubes and Metal Nanowires. *Appl. Phys. Lett.* **2006**, *89*, 243122.
13. Meng, G. W.; Han, F. M.; Zhao, X. L.; Chen, B. S.; Yang, D. C.; Liu, J. X.; Xu, Q. L.; Kong, M. G.; Zhu, X. G.; Jung, Y. J.; *et al.* A General Synthetic Approach to Interconnected Nanowire/Nanotube and Nanotube/Nanowire/Nanotube Heterojunctions with Branched Topology. *Angew. Chem., Int. Ed.* **2009**, *48*, 7166–7170.
14. Seifert, G.; Kohler, T.; Urbassek, H. M.; Hernandez, E.; Frauenheim, T. Tubular Structures of Silicon. *Phys. Rev. B* **2001**, *63*, 193409.
15. Singh, A. K.; Briere, T. M.; Kumar, V.; Kawazoe, Y. Magnetism in Transition-Metal-Doped Silicon Nanotubes. *Phys. Rev. Lett.* **2003**, *91*, 146802.
16. Ni, M.; Luo, G. F.; Lu, J.; Lai, L.; Wang, L.; Jing, M. W.; Song, W.; Gao, Z. X.; Li, G. P.; Mei, W. N.; *et al.* First-Principles Study of Hydrogen-Passivated Single-Crystalline Silicon Nanotubes: Electronic and Optical Properties. *Nanotechnology* **2007**, *18*, 505707.
17. Bai, J.; Zeng, X. C.; Tanaka, H.; Zeng, J. Y. Metallic Single-Walled Silicon Nanotubes. *Proc. Natl. Acad. Sci. U.S.A.* **2004**, *101*, 2664–2668.
18. Lan, J. H.; Cheng, D. J.; Cao, D. P.; Wang, W. C. Silicon Nanotube as a Promising Candidate for Hydrogen Storage: From the First Principle Calculations to Grand Canonical Monte Carlo Simulations. *J. Phys. Chem. C* **2008**, *112*, 5598–5604.
19. Homma, Y.; Kobayashi, Y.; Ogino, T.; Takagi, D.; Ito, R.; Jung, Y. J.; Ajayan, P. M. Role of Transition Metal Catalysts in Single-Walled Carbon Nanotube Growth in Chemical Vapor Deposition. *J. Phys. Chem. B* **2003**, *107*, 12161–12164.
20. Fagan, S. B.; Baierle, R. J.; Mota, R.; da Silva, A. J. R.; Fazzio, A. *Ab Initio* Calculations for a Hypothetical Material: Silicon Nanotubes. *Phys. Rev. B* **2000**, *61*, 9994–9996.
21. Chen, Y. W.; Tang, Y. H.; Pei, L. Z.; Guo, C. Self-Assembled Silicon Nanotubes Grown from Silicon Monoxide. *Adv. Mater.* **2005**, *17*, 564–567.
22. Sha, J.; Niu, J. J.; Ma, X. Y.; Xu, J.; Zhang, X. B.; Yang, Q.; Yang, D. Silicon Nanotubes. *Adv. Mater.* **2002**, *14*, 1219–1221.
23. Jeong, S. Y.; Kim, J. Y.; Yang, H. D.; Yoon, B. N.; Choi, S. H.; Kang, H. K.; Yang, C. W.; Lee, Y. H. Synthesis of Silicon Nanotubes on Porous Alumina Using Molecular Beam Epitaxy. *Adv. Mater.* **2003**, *15*, 1172–1176.
24. Mu, C.; Yu, Y. X.; Liao, W.; Zhao, X. S.; Xu, D. S.; Chen, X. H.; Yu, D. P. Controlling Growth and Field Emission Properties of Silicon Nanotube Arrays by Multistep Template Replication and Chemical Vapor Deposition. *Appl. Phys. Lett.* **2005**, *87*, 113104.
25. Hu, J. Q.; Bando, Y.; Liu, Z. W.; Zhan, J. H.; Golberg, D.; Sekiguchi, T. Synthesis of Crystalline Silicon Tubular Nanostructures with ZnS Nanowires as Removable Templates. *Angew. Chem., Int. Ed.* **2004**, *43*, 63–66.
26. Huang, Z. F.; Harris, K. D.; Brett, M. J. Morphology Control of Nanotube Arrays. *Adv. Mater.* **2009**, *21*, 2983–2987.
27. She, J. C.; An, S.; Deng, S. Z.; Chen, J.; Xiao, Z. M.; Zhou, J.; Xu, N. S. Laser Welding of a Single Tungsten Oxide Nanotip on a Handleable Tungsten Wire: A Demonstration of Laser-Weld Nanoassembly. *Appl. Phys. Lett.* **2007**, *90*, 073103.
28. Peng, Y.; Cullis, T.; Inkson, B. Bottom-up Nanoconstruction by the Welding of Individual Metallic Nanoobjects Using Nanoscale Solder. *Nano Lett.* **2009**, *9*, 91–96.
29. Sui, Y. C.; Cui, B. Z.; Martinez, L.; Perez, R.; Sellmyer, D. J. Pore Structure, Barrier Layer Topography and Matrix Alumina Structure of Porous Anodic Alumina Film. *Thin Solid Films* **2002**, *406*, 64–69.
30. Xu, Q. L.; Meng, G. W.; Han, F. M.; Zhao, X. L.; Kong, M. G.;

Zhu, X. G. Controlled Fabrication of Gold and Polypyrrole Nanowires with Straight and Branched Morphologies *via* Porous Alumina Template-Assisted Approach. *Mater. Lett.* **2009**, *63*, 1431–1434.
31. Meng, G. W.; Jung, Y. J.; Cao, A. Y.; Vajtai, R; Ajayan, P. M. Controlled Fabrication of Hierarchically Branched Nanopores, Nanotubes, and Nanowires. *Proc. Natl. Acad. Sci. U.S.A.* **2005**, *102*, 7074–7078.
32. Huang, Y.; Duan, X. F.; Cui, Y.; Lauhon, L. J.; Kim, K. H.; Lieber, C. M. Logic Gates and Computation from Assembled Nanowire Building Blocks. *Science* **2001**, *294*, 1313–1317.
33. Papadopoulos, C.; Rakitin, A.; Li, J.; Vedeneev, A. S.; Xu, J. M. Electronic Transport in Y-Junction Carbon Nanotubes. *Phys. Rev. Lett.* **2000**, *85*, 3476–3479.
34. Masuda, H.; Fukuda, K. Ordered Matal Nanohole Arrays Made by a 2-Step Replication of Honeycomb Structures of Anodic Alumina. *Science* **1995**, *268*, 1466–1468.
35. Qin, D. H.; Lu, M.; Li, H. L. Magnetic Force Microscopy of Magnetic Domain Structure in Highly Ordered Co Nanowire Arrays. *Chem. Phys. Lett.* **2001**, *350*, 51–56.